Received: 15 October 2015 | Revised: 28 April 2016 | Accepted: 17 September 2016

DOI 10.1002/nla.2074

WILEY

RESEARCH ARTICLE

On an Uzawa smoother in multigrid for poroelasticity equations

P. Luo[1] | C. Rodrigo[2] | F. J. Gaspar[3] | C. W. Oosterlee[1,3]

[1]DIAM, Delft University of Technology, Netherlands
[2]Department of Applied Mathematics, University of Zaragoza, Spain
[3]CWI, Centrum Wiskunde and Informatica, Amsterdam, Netherlands

Correspondence
P. Luo, DIAM, Delft University of Technology, Mekelweg 4, 2628 CD, Delft, The Netherlands.
Email: p.luo@tudelft.nl

Funding information
China Scholarship Council (CSC), NDNS+PhD travel grant, DGA (Grupo consolidado PDIE), Grant/Award Number: FEDER/MCYT Projects MTM2013-40842-P, European Union's Horizon 2020 research and innovation programme under the Marie Sklodowska-Curie, Grant/Award Number: 705402, POROSOS.

Summary

A poroelastic saturated medium can be modeled by means of Biot's theory of consolidation. It describes the time-dependent interaction between the deformation of porous material and the fluid flow inside of it. Here, for the efficient solution of the poroelastic equations, a multigrid method is employed with an Uzawa-type iteration as the smoother. The Uzawa smoother is an equation-wise procedure. It shall be interpreted as a combination of the symmetric Gauss-Seidel smoothing for displacements, together with a Richardson iteration for the Schur complement in the pressure field. The Richardson iteration involves a relaxation parameter which affects the convergence speed, and has to be carefully determined. The analysis of the smoother is based on the framework of local Fourier analysis (LFA) and it allows us to provide an analytic bound of the smoothing factor of the Uzawa smoother as well as an optimal value of the relaxation parameter. Numerical experiments show that our upper bound provides a satisfactory estimate of the exact smoothing factor, and the selected relaxation parameter is optimal. In order to improve the convergence performance, the acceleration of multigrid by iterant recombination is taken into account. Numerical results confirm the efficiency and robustness of the acceleration scheme.

KEYWORDS

heterogeneity, iterant recombination scheme, local Fourier analysis, multigrid method, poroelasticity, Uzawa smoother

1 | INTRODUCTION

The concept of poroelasticity describes the behavior of a deformable fluid-saturated porous medium. It is a well-developed theory that was first studied by Terzaghi[1] who proposed a model for a one-dimensional consolidation problem. Biot[2,3] extended the theory to a general three-dimensional model that models the interaction between the solid deformation and the fluid motion. Usually, there are two basic phenomena regarding poroelastic behavior. One is the 'solid to fluid coupling' which means that a change in the applied stresses of the skeleton will affect the pressure or mass of the fluid. The other is the 'fluid to solid coupling' when a change in the fluid will lead to a change in the volume of the material.

The multigrid method – an efficient numerical technique for systems of linear and nonlinear equations, is employed for solving the discretized poroelastic partial differential equations. An important multigrid component is the smoother, and the performance of multigrid crucially depends on it. There are several branches of robust smoothers developed for the poroelasticity equations. They all fall into two major categories: coupled and decoupled smoothers, see.[4–6] With respect to the coupled smoothers, the Vanka smoother,[7] which is sometimes called box relaxation, was originally proposed for solving the Navier-Stokes equations discretized by finite differences. This approach locally couples some unknowns occurring in the equations and can be applied to a wide range of problems. Decoupled smoothers, that is,

equation-wise relaxations, are popular due to their convenient implementation and efficiency. Here, we focus on a specific type of decoupled smoothers called Uzawa smoothers, for different discretizations of the poroelasticity problem.

A first study of the Uzawa smoother was done in the PhD thesis, as well as in a conference proceedings paper, by P. Nigon.[8] A symmetric Gauss-Seidel (SGS) smoother will be employed here for the displacement variables. In,[8] two forward Gauss-Seidel sweeps were used instead, but numerical results in[9] revealed that, everything else being equal, the SGS choice is indeed more effective. In addition, for the pressure unknowns, the Uzawa method shall be interpreted as a Richardson iteration for solving the Schur complement equation in which a relaxation parameter is involved. Optimization of this parameter is necessary for fast multigrid convergence. Detailed research of this method for a family of Stokes problems has already been done in.[9]

A suitable relaxation parameter is chosen by means of local Fourier analysis (LFA).[10] LFA is a powerful tool for the quantitative analysis of the convergence of multigrid. The idea was first proposed by Brandt[11] in 1977 and then developed and refined in.[12] A systematic introduction can be found in the books by Wesseling,[13] and Trottenberg et al.[10] Particularly, a software package for LFA provided by Wienands and Joppich[14] is useful for practical experiments. In this paper, we are concerned with the convergence behavior of multigrid with the Uzawa smoother with respect to relaxation parameters and the poroelastic model's coefficients. We get an upper bound for the smoothing factor and a concrete formulation of the relaxation parameter which is governed by the main problem coefficients. We consider both staggered and collocated finite volume discretizations of poroelasticity equations in our analysis for which we find different relaxation parameters. In order to confirm our study, several numerical tests are performed.

We are also interested in heterogeneous poroelasticity problems. Heterogeneity means that coefficients in the equations are not constant but follow some distribution. For the heterogeneous case, the same multigrid method with Uzawa smoother is applied, however, the convergence performance will be influenced by the anisotropy. To improve the convergence, the so-called acceleration of multigrid by an iterant recombination scheme[10] is taken into account. In practice, this leads to a similar algorithm as a multigrid preconditioning method. Different numerical experiments validate the efficiency and robustness of the acceleration scheme.

The organization of the paper is as follows. We present the incompressible poroelasticity equations in Section 2. The numerical method is introduced in Section 3. In Section 4, we analyze the proposed smoother in the framework of LFA. We obtain an analytic bound of the smoothing factor. After that, the multigrid method is applied to both staggered and collocated grids. Numerical experiments illustrate the efficiency of the method and confirm our analysis in Section 5. Acceleration of multigrid by the iterant recombination scheme is employed for the heterogeneous poroelasticity system. Finally, conclusions are drawn in Section 6.

2 | PROBLEM FORMULATION

2.1 | Poroelasticity equations

We consider the quasi-static Biot model for soil consolidation. The porous medium is assumed to be linearly elastic, homogeneous and isotropic, and the porous matrix is supposed to be saturated by an incompressible Newtonian fluid. The continuous medium is characterized by the knowledge of elastic displacements $\mathbf{u} = (u,v)$, and fluid pressure p at each point, and in terms of these unknowns the governing equations of the consolidation problem are given by

$$-\nabla \cdot G\nabla \mathbf{u} - \nabla(\lambda + G)(\nabla \cdot \mathbf{u}) + \nabla p = \mathbf{g}(\mathbf{x}, t), \qquad (1)$$

$$\frac{\partial}{\partial t}(\nabla \cdot \mathbf{u}) - \nabla \cdot \left(\frac{k}{\eta}\nabla\, p\right) = f(\mathbf{x}, t), \quad \mathbf{x} \in \Omega, 0 < t \leq T, \qquad (2)$$

where λ and G are the Lamé coefficients, which can be computed from the values of the Young modulus E and the Poisson ratio ν in the following way,

$$\lambda = \frac{\nu E}{(1+\nu)(1-2\nu)}, \quad G = \frac{E}{2(1+\nu)}, \qquad (3)$$

k is the permeability of the porous medium and η is the viscosity of the fluid. The source terms $\mathbf{g}(\mathbf{x},t)$ and $f(\mathbf{x},t)$ represent a density of applied body forces and a forced fluid extraction or injection process, respectively. The following initial condition is assumed,

$$\nabla \cdot \mathbf{u}\,(\mathbf{x}, 0) = 0, \quad \mathbf{x} \in \Omega.$$

For simplicity, we will consider homogeneous Dirichlet boundary conditions for both displacements and pressure, $\mathbf{u} = \mathbf{0}$ and $p = 0$ on $\partial\Omega$.

Whatever the chosen space discretization scheme and an implicit scheme in time, the discretization of 1–2 leads at each time step to a linear system of the form

$$\begin{pmatrix} A & B^T \\ B & -C \end{pmatrix} \begin{pmatrix} \mathbf{u} \\ p \end{pmatrix} = \begin{pmatrix} \mathbf{g} \\ f \end{pmatrix}, \qquad (4)$$

where A is the discrete representation of the elasticity operator $-\nabla \cdot G\nabla\,\mathbf{u} - \nabla(\lambda + G)\,(\nabla \cdot \mathbf{u})$. It follows that A is symmetric positive definite (SPD). The matrix block B^T is the discrete gradient and B the negative discrete divergence; C contains the term $-\nabla \cdot (\frac{k}{\eta}\nabla p)$ and also it can contain a stabilization term that is needed for some discretization schemes to avoid spurious oscillations. Notice that in practice operator C is an almost zero block because the permeability k is very small and also this block contains the time-discretization parameter as a multiplicative factor, which can also be arbitrarily small.

2.2 | Discretization

Discretization on staggered grids In a staggered arrangement of the poroelasticity equations, the discrete values of u_h and v_h, the components of the displacement vector, are located at the grid cell faces in the •– and ∘–points, respectively,

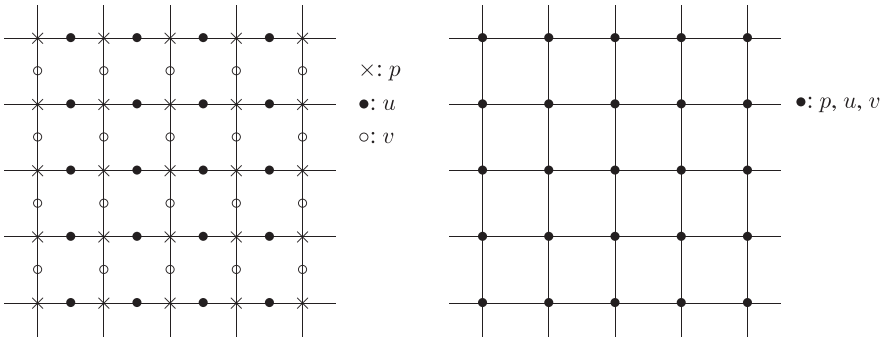

FIGURE 1 Staggered (left) and collocated (right) grid location of unknowns for poroelasticity equations.

and the discrete pressure unknowns p_h are defined at the grid points (the $\times$–points), as in poroelasticity applications pressure values are often prescribed at the boundary, see Figure 1 (left side).

For each equation, the discretization is centered around the equation's primary unknown. On a staggered grid, the stencil form in the case of constant coefficients and the finite volume scheme typically results in the following:

$$\begin{bmatrix} & -G & \\ -(\lambda+2G) & 2(\lambda+3G) & -(\lambda+2G) \\ & -G & \end{bmatrix} u_h - (\lambda+G) \begin{bmatrix} -1 & & 1 \\ & \star & \\ 1 & & -1 \end{bmatrix} v_h + h \begin{bmatrix} -1 & \star & 1 \end{bmatrix} p_h = g_h^1 h^2, \tag{5}$$

$$-(\lambda+G) \begin{bmatrix} -1 & & 1 \\ & \star & \\ 1 & & -1 \end{bmatrix} u_h + \begin{bmatrix} & -(\lambda+2G) & \\ -G & 2(\lambda+3G) & -G \\ & -(\lambda+2G) & \end{bmatrix} v_h + h \begin{bmatrix} 1 \\ \star \\ -1 \end{bmatrix} p_h = g_h^2 h^2, \tag{6}$$

$$h \begin{bmatrix} -1 & \star & 1 \end{bmatrix} u_h + h \begin{bmatrix} 1 \\ \star \\ -1 \end{bmatrix} v_h + \kappa \begin{bmatrix} & -1 & \\ -1 & 4 & -1 \\ & -1 & \end{bmatrix} p_h = f_h h^2, \tag{7}$$

where $\kappa = \frac{k\Delta t}{\eta}$, with Δt the time step. The $\star$ denotes the position on the grid at which the discrete operator is applied, that is, $\bullet$, $\circ$ or $\times$ - points, respectively.

Discretization on collocated grids We also consider the vertex-centered finite volume discretization of the poroelastic system on a collocated grid. We assume a uniform grid of cells of size h. In a collocated grid all variables are placed at the grid points, see Figure 1 (right side).

Collocated grid arrangements are convenient for grid generation and also for numerical methods like multigrid. However, when a standard collocated discretization is used for the poroelasticity problem, non-physical oscillations can appear in the pressure field approximation of the numerical solution.[4,5] To avoid this, a stabilization term has to be added to the flow equation 2. A stable discretization was proposed in.[4] In this way, matrix C in 4 contains an artificial term, that is,

$$-C = \nabla \cdot (\kappa \nabla) + \nabla \cdot \left(\frac{h^2}{4(\lambda+2G)} \nabla \right). \tag{8}$$

Because the stabilization term is proportional to h^2, second order accuracy is maintained if all terms in the system are discretized with second order accuracy.

3 | THE NUMERICAL METHOD

3.1 | Multigrid and acceleration by iterant recombination

With respect to the numerical solution method, multigrid is considered for the discrete poroelasticity problems due to its efficiency and robustness. The multigrid method is based on two crucial components. One is the relaxation method (the smoother), the other is the coarse grid correction. Regarding the coarse grid correction, geometric grid coarsening is chosen as we will deal with regular Cartesian grids here. The sequence of coarse grids is obtained by doubling the mesh size in each spatial direction.

For the staggered case, the inter-grid transfer operators that act on the different unknowns are defined as follows: At $u-$ and $v-$ grid points one considers 6-point restrictions and at p-grid points a 9-point vertex-centered full weighting restriction is applied. In stencil notation, the restriction operators are given by

$$R_{h,2h}^u = \frac{1}{8} \begin{pmatrix} 1 & & 1 \\ 2 & * & 2 \\ 1 & & 1 \end{pmatrix}_h,$$

$$R_{h,2h}^v = \frac{1}{8} \begin{pmatrix} 1 & 2 & 1 \\ & * & \\ 1 & 2 & 1 \end{pmatrix}_h,$$

$$R_{h,2h}^p = \frac{1}{16} \begin{pmatrix} 1 & 2 & 1 \\ 2 & 4 & 2 \\ 1 & 2 & 1 \end{pmatrix}_h,$$

respectively. As the prolongation operators $P_{2h,h}^{u/v/p}$, one applies the usual interpolation operators based on bilinear interpolation of neighboring coarse grid unknowns on the staggered grid.

For the collocated case, the multigrid transfer operators, restriction $R_{h,2h}$, and prolongation $P_{2h,h}$, are well known in geometric multigrid. In a standard way, the full-weighting

restriction and the bilinear interpolation are applied as the inter-grid transfer operators, see, ([10] Chapter 2).

The choice of smoother, which has a great effect on the behavior of a multigrid method, needs to be done with special attention. The Uzawa smoother which is discussed in detail in the next section, is chosen here due to the fact that it is a simple algorithm with low computational cost.

To improve the multigrid performance, we also consider an acceleration scheme. The acceleration of multigrid means that multigrid is applied as a preconditioner in connection with a Krylov subspace method. As is known, a Krylov acceleration technique helps to capture eigenvectors connected to the isolated large eigenvalues of the iteration matrix. These eigenvectors are the main reason for limited multigrid convergence in some specific situations. For detailed information, see.[15]

From the multigrid point of view, multigrid as a preconditioner is identical to multigrid acceleration by iterant recombination. [[10], Section 7.8] The technique of iterant recombination is easily implemented on both staggered and collocated grids, and can also be used in the nonlinear case. This algorithm will be described shortly.

Supposing we already had successive approximations $\mathbf{w}_h^1, \mathbf{w}_h^2, \dots, \mathbf{w}_h^q$ with $\mathbf{w}_h^i = (\mathbf{u}_h^i, p_h^i), i = 1, \dots, q$, and corresponding residuals $\mathbf{r}_h^1, \mathbf{r}_h^2, \dots, \mathbf{r}_h^q$ from previous multigrid cycles. For the sake of a more optimal approximation of the solution $\mathbf{w}_{h,new}$, a linear combination of the $\tilde{q}+1$ ($\tilde{q} < q$), recent intermediate approximations $\mathbf{w}_h^{q-i}, i = 0, \dots, \tilde{q}$, is considered,

$$\mathbf{w}_{h,new} = \mathbf{w}_h^q + \sum_{i=1}^{\tilde{q}} \alpha_i \left(\mathbf{w}_h^{q-i} - \mathbf{w}_h^q \right). \tag{9}$$

For linear problems, the improved residual will have the same form as 9,

$$\mathbf{r}_{h,new} = \mathbf{r}_h^q + \sum_{i=1}^{\tilde{q}} \alpha_i \left(\mathbf{r}_h^{q-i} - \mathbf{r}_h^q \right). \tag{10}$$

In order to select an optimal candidate $\mathbf{w}_{h,new}$ for the solution, the parameters α_i are required to minimize the residual 10, for example, with respect to the $L_2 -$ norm $\|\cdot\|_2$.

The acceleration of multigrid is transferred to a classical minimization problem. Usually, we search for the desired coefficients α_i through a (Gram-Schmidt) orthonormalization process. The structure of a multigrid V-cycle with the acceleration by iterant recombination is presented in Figure 2. We will particularly employ the acceleration for the heterogeneous poroelastic cases, for which it may be nontrivial to define an optimal multigrid solver.

3.2 | The Uzawa smoother

Here, we are interested in a decoupled Uzawa smoother which was analyzed for Stokes problems in fluid dynamics in.[9]

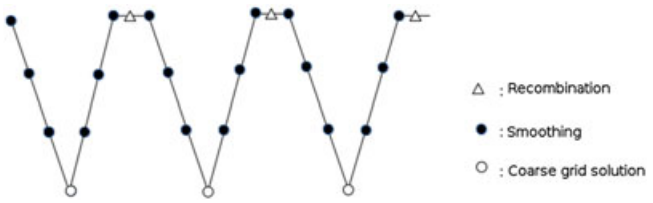

FIGURE 2 Recombination of multigrid iterants.

The smoother is obtained by splitting the discrete operator as follows

$$\begin{pmatrix} A & B^T \\ B & -C \end{pmatrix} = \begin{pmatrix} M_A & \\ B & -\omega^{-1} I \end{pmatrix} - \begin{pmatrix} M_A - A & -B^T \\ & C - \omega^{-1} I \end{pmatrix}, \tag{11}$$

where M_A is a typical smoother for A and ω is some positive parameter. M_A helps to make the approach less costly because of the inexact solve for displacements at each iteration.

Supposing we already got an approximation of the solution $(\mathbf{u},p)^T$ to the system, the relaxed approximation $(\hat{\mathbf{u}},\hat{p})^T$ is computed according to the decoupled Uzawa smoother as

$$\begin{pmatrix} M_A & \\ B & -\omega^{-1} I \end{pmatrix} \begin{pmatrix} \hat{\mathbf{u}} \\ \hat{p} \end{pmatrix} = \begin{pmatrix} M_A - A & -B^T \\ & C - \omega^{-1} I \end{pmatrix} \begin{pmatrix} \mathbf{u} \\ p \end{pmatrix} + \begin{pmatrix} \mathbf{g} \\ f \end{pmatrix}. \tag{12}$$

A single step of the iteration is described as

- Relax the displacements by applying M_A: $\hat{\mathbf{u}} = \mathbf{u} + M_A^{-1}\left(\mathbf{g} - A\mathbf{u} - B^T p\right)$;
- Update the pressure: $\hat{p} = p + \omega(B\hat{\mathbf{u}} - Cp - f)$.

Here, the SGS method is considered as M_A, which consists of one forward and one backward sweep for all displacements in the computational domain. M_A has two important properties used in our theoretical analysis. One is that M_A is SPD if A is SPD. The other is that the associated largest eigenvalue satisfies (see, e.g., [[16], Theorem 7.17])

$$\lambda_{\max}(M_A^{-1}A) \quad \leq \quad 1. \tag{13}$$

4 | LOCAL FOURIER ANALYSIS

The Uzawa smoother is analyzed by means of LFA. In particular, we aim to define an optimal ω in 12. We assume the parameters λ,G, and κ are constants here.

4.1 | Basis of LFA

In LFA, it is assumed that the discrete operator is defined on an infinite grid $\mathcal{G}_h$, and boundary conditions are neglected. For example, an infinite collocated grid in 2D can be defined as

$$\mathcal{G}_h = \{\boldsymbol{x} = \boldsymbol{kh} := (k_1 h_1, k_2 h_2), \quad \boldsymbol{k} \in \mathbb{Z}^2\}, \tag{14}$$

where we denote $\boldsymbol{x} = (x_1, x_2) \in \mathcal{G}_h$ and $\boldsymbol{h} = (h_1, h_2)$. The basic idea of LFA is that all occurring multigrid components, the discrete approximation and its corresponding error or residual can be represented by linear combinations of Fourier modes, defined in the case of a collocated grid as

$$\varphi_h(\boldsymbol{\theta}, \boldsymbol{x}) = e^{i\boldsymbol{\theta}\cdot\boldsymbol{x}/\boldsymbol{h}} := e^{i\theta_1 x_1/h_1} e^{i\theta_2 x_2/h_2}, \tag{15}$$

where $\boldsymbol{\theta} \in \boldsymbol{\Theta} := (-\pi, \pi]^2$, which form a unitary basis of the space of infinite grid functions. The Fourier space generated by Fourier modes is given by

$$\mathcal{F}(\mathcal{G}_h) := \text{span}\{\varphi_h(\boldsymbol{\theta}, \cdot) | \boldsymbol{\theta} \in \boldsymbol{\Theta}\}. \tag{16}$$

For the analysis, we distinguish high and low frequency components on $\mathcal{G}_h$,

$$\boldsymbol{\Theta}^{2h}_{low} := \left(-\frac{\pi}{2}, \frac{\pi}{2}\right]^2, \qquad \boldsymbol{\Theta}^{2h}_{high} := \boldsymbol{\Theta} \setminus \Theta^{2h}_{low}. \tag{17}$$

In multigrid, the purpose of the smoother is to eliminate the high frequency components of an error, whereas the low frequency ones are typically reduced by coarse grid correction. In our case, the Uzawa smoothing iteration can be written as $Q_h = I - M_h^{-1} K_h$, where K_h and M_h are the matrices of systems 4 and 12, respectively. To study how the high frequency components are eliminated, we define the smoothing factor μ as:

$$\mu = \sup_{\boldsymbol{\theta} \in \boldsymbol{\Theta}^{2h}_{high}} \rho(Q_h(\boldsymbol{\theta})). \tag{18}$$

In the transition from $\mathcal{G}_h$ to $\mathcal{G}_{2h}$, each low-frequency $\boldsymbol{\theta} = \boldsymbol{\theta}^{00} \in \boldsymbol{\Theta}^{2h}_{low}$ is coupled with three high-frequencies $\boldsymbol{\theta}^{11}, \boldsymbol{\theta}^{10}, \boldsymbol{\theta}^{01}$, given by

$$\boldsymbol{\theta}^{ij} = \theta^{00} - (i\ sign(\theta_1), j\ sign(\theta_2))\pi, \quad i, j = 0, 1. \tag{19}$$

Only low frequency components are distinguishable on the coarse grid $\mathcal{G}_{2h}$. In other words, for each θ^{00}, three other Fourier modes $\phi_{2h}(\theta^{11}, \cdot), \phi_{2h}(\theta^{10}, \cdot)$, and $\phi_{2h}(\theta^{01}, \cdot)$ are identical to $\phi_{2h}(\theta^{00}, \cdot)$ on $\mathcal{G}_{2h}$. This means they are invisible on the coarse grid. As a result, the Fourier space is subdivided into corresponding four-dimensional subspaces, known as $2h$-harmonics,

$$\mathcal{F}^{2h}(\boldsymbol{\theta}) := \text{span}\{\boldsymbol{\phi}_h(\boldsymbol{\theta}^{00}, \cdot), \boldsymbol{\phi}_h(\boldsymbol{\theta}^{11}, \cdot), \boldsymbol{\phi}_h(\boldsymbol{\theta}^{10}, \cdot), \boldsymbol{\phi}_h(\boldsymbol{\theta}^{01}, \cdot)\}, \quad \text{with} \quad \boldsymbol{\theta} = \boldsymbol{\theta}^{00} \in \Theta^{2h}_{low}. \tag{20}$$

By the definitions above, we can analyze the behavior of multigrid by investigating the effect of the multigrid components acting on the Fourier space.

In a two-grid analysis, it is assumed that the coarse grid solution is exact on the first coarser grid level. The iteration operator of the two-grid method is given by

$$M_{h,2h} = Q_h^{\nu_2}(I_h - P_{2h,h}(K_{2h})^{-1} R_{h,2h} K_h) Q_h^{\nu_1}, \tag{21}$$

where ν_1, ν_2 are, respectively, the number of pre- and post-smoothing steps. Because the representation of $M_{h,2h}$ on the Fourier space has a block-diagonal structure regarding the partitioning in $2h$-harmonics, it is possible to efficiently calculate the LFA two-grid convergence factor,

$$\rho = \rho(M_{h,2h}). \tag{22}$$

For the staggered case, the definition of the infinite grid and as a consequence the definition of the Fourier modes are different, what makes the analysis more involved, see[14,17] for details.

4.2 | LFA for the Uzawa smoother

A LFA for the considered Uzawa smoother was already developed in.[9] In particular, the authors provided an upper bound on the smoothing factor associated with the proposed Uzawa smoother which gave an excellent estimate of the exact smoothing factor. More concretely, this bound was given by

$$\mu \leq \bar{\mu} = \max\left((\mu_A)^{1/2}, \mu_S\right), \tag{23}$$

where μ_A is the smoothing factor corresponding to the relaxation scheme M_A, and μ_S can be interpreted as the smoothing factor associated with the Richardson iteration for the Schur complement,

$$\mu_S := \sup_{\boldsymbol{\Theta}^{2h}_{high}} \rho\left(I - \omega\left(C + BA^{-1}B^T\right)\right).$$

In order to bound μ_A, available results in the literature were used from scalar elliptic PDEs. Notice that in our case also the smoothing factors of several smoothers for the elasticity operator are well-known. However, bounding μ_S is more involved because the eigenvalues of the Schur complement contribute to the analysis of this smoothing factor. In addition to that, the information of these eigenvalues plays an important role in selecting the relaxation parameter for the Richardson iteration. In,[9] a detailed study of the maximum and minimum eigenvalues of the Schur complement gave rise to the following bound of μ_S:

$$\mu_S \leq \max\left(\tau - 1, 1 - \frac{\tau}{\kappa_\beta}\right), \tag{24}$$

where

$$\kappa_\beta = \frac{\beta_{\max}}{\beta_{\min}}, \tag{25}$$

with $\beta_{\max}$ and $\beta_{\min}$ the following eigenvalue bounds,

$$\max_{\boldsymbol{\theta} \in \Theta^{2h}_{high}} \left(\tilde{C}(\boldsymbol{\theta}) + \tilde{B}(\boldsymbol{\theta})\widetilde{A^{-1}}(\boldsymbol{\theta})\widetilde{B^T}(\boldsymbol{\theta})\right) = \beta_{\max}, \tag{26}$$

$$\min_{\boldsymbol{\theta} \in \Theta^{2h}_{high}} \left(\tilde{C}(\boldsymbol{\theta}) + \tilde{B}(\boldsymbol{\theta})\widetilde{A^{-1}}(\boldsymbol{\theta})\widetilde{B^T}(\boldsymbol{\theta})\right) = \beta_{\min}, \tag{27}$$

with $\tilde{C}(\boldsymbol{\theta}), \tilde{B}(\boldsymbol{\theta}), \widetilde{A^{-1}}(\boldsymbol{\theta})$ and $\widetilde{B^T}(\boldsymbol{\theta})$ the symbols or Fourier representations of operators C, B, A^{-1} and B^T for a fixed frequency $\boldsymbol{\theta}$, and where τ is a positive real number such as $\tau < 2$ (to ensure that $\mu_S < 1$). This analysis resulted in a formula to determine the appropriate relaxation parameter as (see,[9] Theorem 3.2)

$$\omega = \frac{\tau}{\beta_{\max}} = \frac{2}{\beta_{\max} + \beta_{\min}}, \tag{28}$$

where τ was chosen to minimize the value of the maximum in 24. All these results can be extrapolated to the analysis of the Uzawa smoother for the poroelasticity equations that we consider here, and in the next section we will provide exact values for the bounds of the eigenvalues which will give us optimal relaxation parameters for different discretizations of our problem.

5 | UZAWA BASED MULTIGRID FOR POROELASTICITY EQUATIONS

We will work out the smoothing analysis from the previous section for staggered and collocated poroelasticity discretizations.

5.1 | Staggered grid arrangement of unknowns

Theoretical analysis. For the staggered discretization of the poroelastic equations, a geometric multigrid is adopted. The Uzawa smoother can be applied, and we can perform the theoretical analysis explained in Section 4.2 in order to obtain a suitable parameter ω for the part corresponding to the Richardson iteration for the pressure.

To obtain $\beta_{\max}(h)$ and $\beta_{\min}(h)$, in 26 and 27, we will take into account the following equalities which are valid only for the staggered arrangement

$$\tilde{B}(\boldsymbol{\theta})\tilde{\mathrm{A}}(\boldsymbol{\theta}) = -(\lambda + 2G)\tilde{\Delta}(\boldsymbol{\theta})\tilde{B}(\boldsymbol{\theta}), \tag{29}$$

$$\tilde{B}(\boldsymbol{\theta})\widetilde{B^T}(\boldsymbol{\theta}) = -\tilde{\Delta}(\boldsymbol{\theta}), \tag{30}$$

so that

$$\tilde{B}(\boldsymbol{\theta})\widetilde{A^{-1}}(\boldsymbol{\theta})\widetilde{B^T}(\boldsymbol{\theta}) = -\frac{1}{\lambda + 2G}\widetilde{\Delta^{-1}}(\boldsymbol{\theta})\tilde{B}(\boldsymbol{\theta})\widetilde{B^T}(\boldsymbol{\theta}) = \frac{1}{\lambda + 2G}. \tag{31}$$

Denoting $s_1 = \sin^2\left(\frac{\theta_1}{2}\right)$ and $s_2 = \sin^2\left(\frac{\theta_2}{2}\right)$, the symbol of $-\Delta$ for a frequency $\boldsymbol{\theta} = (\theta_1,\theta_2)$ is given by $-\tilde{\Delta}(\boldsymbol{\theta}) = \frac{4}{h^2}(s_1 + s_2)$. Therefore, the symbol of the Schur complement is written as

$$\tilde{C}(\boldsymbol{\theta}) + \tilde{B}(\boldsymbol{\theta})\widetilde{A^{-1}}(\boldsymbol{\theta})\widetilde{B^T}(\boldsymbol{\theta}) = \frac{4\kappa}{h^2}(s_1 + s_2) + \frac{1}{\lambda + 2G}. \tag{32}$$

Then, we obtain

$$\beta_{\max}(h) = \frac{8\kappa}{h^2} + \frac{1}{\lambda + 2G} \quad \text{(achieved for } \theta_1 = \theta_2 = \pi\text{)}, \tag{33}$$

$$\beta_{\min}(h) = \frac{2\kappa}{h^2} + \frac{1}{\lambda + 2G} \quad \text{(achieved for } \theta_1 = 0, \theta_2 = \frac{\pi}{2}\text{)}. \tag{34}$$

With these values, we can write

$$\kappa_\beta = \frac{\beta_{\max}}{\beta_{\min}} = \frac{8\kappa(\lambda + 2G) + h^2}{2\kappa(\lambda + 2G) + h^2}, \tag{35}$$

and when $\kappa = 0$ the simplified expression reads $\kappa_\beta = 1$. We find the value of τ which gives the lowest value of the maximum in 24, resulting in (taking into account that $\tau \leq 2$)

$$\tau = \frac{2\kappa_\beta}{1 + \kappa_\beta} = \frac{8\kappa(\lambda + 2G) + h^2}{5\kappa(\lambda + 2G) + h^2}, \tag{36}$$

and with this value, the smoothing factor is bounded by 0.6, independently of the values of κ and Lamé coefficients λ, G,

$$\mu_S = \frac{3\kappa(\lambda + 2G)}{5\kappa(\lambda + 2G) + h^2} \leq 0.6. \tag{37}$$

Moreover, following 28 the relaxation parameter is given by the expression

$$\omega = \frac{h^2(\lambda + 2G)}{5\kappa(\lambda + 2G) + h^2}. \tag{38}$$

Some results. We would like to quantitatively determine μ_S based on the previous theory. A suitable relaxation parameter ω needs to be selected for the Richardson iteration. To define this ω with the rule 38, we need first to compute $\beta_{\max}(h)$ and $\beta_{\min}(h)$ from 33 and 34. After that, κ_β and τ are obtained via 35, 36.

Table 1 shows the values of the parameters necessary to compute the relaxation parameter and smoothing factor μ_S for different coefficients of κ on the staggered grid. We consider the following values of the Lamé coefficients: $\lambda = 12500$ and $G = 8333$.

The smoothing factor corresponding to the SGS smoother is $\mu_A = 0.4927$ for only one smoothing step. Therefore, $(\mu_A)^{1/2} = 0.70$, which results in a bound of the smoothing factor for the whole system based on inequality 23.

In Table 2, we present the smoothing and two-grid convergence factors for the proposed multigrid method with Uzawa

TABLE 1 Values of the parameters computed by the theory, together with the resulting relaxation parameters ω and smoothing factors μ_S when $h = \frac{1}{256}$ on a staggered grid

Parameters	$\kappa = 1$	$\kappa = 10^{-3}$	$\kappa = 10^{-6}$	$\kappa = 10^{-10}$	$\kappa = 0$
$\beta_{\max}$	5.24×10^5	524.29	0.52	8.67×10^{-5}	3.43×10^{-5}
$\beta_{\min}$	1.31×10^5	131.07	0.13	4.74×10^{-5}	3.43×10^{-5}
κ_β	4	4	4	1.83	1
τ	1.6	1.6	1.6	1.29	1
ω	3.05×10^{-6}	3.10×10^{-3}	3.05	14913	29166
μ_S	0.6	0.6	0.6	0.29	0

TABLE 2 Smoothing and two-grid convergence factors predicted by LFA for different values of κ by using one smoothing step, together with the asymptotic convergence factors experimentally computed

κ	1	10^{-3}	10^{-6}	10^{-10}	0
μ	0.60	0.61	0.60	0.52	0.50
ρ (ρ_h)	0.60 (0.59)	0.61 (0.60)	0.60 (0.59)	0.48 (0.54)	0.61 (0.57)

smoother for different values of κ and considering only one smoothing step. Also, the asymptotic convergence factor ρ_h, experimentally obtained, is shown in the table. Homogeneous Dirichlet boundary conditions are applied and the right hand sides of the poroelasticity equations are all set to zero, so that we can iterate until the asymptotic convergence factor is reached. All results are based on the relaxation parameter ω given in Table 1.

Numerical computation shows that the asymptotic multigrid convergence factor is accurately predicted by the LFA two-grid convergence factor. Regarding the smoothing factor, we obtained an upper bound for all cases.

Remark 1. A well-known challenge for poroelasticity equations is to consider incompressible materials, when the Poisson ratio is close to 0.5. As can be seen from formula 37, the smoothing factor μ_S is bounded by 0.6, independently of all physical parameters. However, it is known that standard smoothers, like the one considered here, for elasticity operator do not give satisfactory results in the incompressible case, because it is a grad-div dominating problem. For this case, more suitable smoothers, as for example the distributive relaxation proposed in,[18] should be used.

The presented analysis can be adapted to the case of non-square meshes, and the corresponding results are shown in Appendix A.1.

Comparison with Vanka smoother In order to support the choice of the proposed Uzawa smoother, in Table 3 for a finest grid with $h = \frac{1}{256}$, we observe that its convergence rate is comparable to that of the Vanka smoother, which has been widely used for saddle point problems and for poroelasticity equations. A relaxation parameter $\omega = 0.7$ is used for the Vanka smoother to perform a fair comparison, because this parameter provides the best multigrid convergence with this smoother. In Table 3, for different values of permeability and numbers of smoothing steps, the number of multigrid iterations to reduce the maximum norm of the residual by 10^{-10} are presented. Whereas the number of iterations is comparable, the Uzawa smoother has a lower computational cost.

Three-dimensional case The analysis performed in the two-dimensional case can be straightforwardly extended to the three dimensional case. In particular, it is easy to derive $\beta_{\max}(h) = \frac{12\kappa}{h^2} + \frac{1}{\lambda+2G}$ and $\beta_{\min}(h) = \frac{2\kappa}{h^2} + \frac{1}{\lambda+2G}$. As a consequence, the bound for the smoothing factor is $\mu_S \leq \frac{5}{7}$, if the optimal value $\omega = \frac{2}{\beta_{\max}+\beta_{\min}}$ is chosen. The LFA smoothing and two-grid convergence factors are displayed in Table 4 for different values of permeability and smoothing steps. The numerically obtained asymptotic convergence factors are also included to validate the LFA results.

TABLE 3 Number of multigrid iterations necessary to reduce the initial residual by a factor of 10^{-10}

smoothing steps	smoother	$\kappa = 10^{-2}$	$\kappa = 10^{-6}$	$\kappa = 10^{-10}$	$\kappa = 0$
1	Vanka	30	30	31	31
	Uzawa	32	32	28	35
2	Vanka	16	16	16	17
	Uzawa	17	17	15	18
3	Vanka	11	11	12	14
	Uzawa	12	12	11	13
4	Vanka	9	9	11	12
	Uzawa	10	10	9	10

5.2 | Collocated grid arrangement of unknowns

Theoretical analysis. Next, we consider the multigrid method with Uzawa smoother for the poroelastic system of equations discretized on a collocated grid. In this case, we also determine the optimal ω-value by the theoretical results in Section 4.2. For this purpose, we first need to get bounds of the eigenvalues of the Schur complement.

The theoretical analysis for the collocated grid is more involved than the staggered case, because equalities 29 and 30 do not hold in the collocated case and therefore we need to follow a different strategy. We rewrite the symbol of the elasticity operator as follows,

$$\begin{aligned}\tilde{A}(\boldsymbol{\theta}) &= (\lambda+G)\tilde{Y}(\boldsymbol{\theta}) = (\lambda+G)(\tilde{N}(\boldsymbol{\theta}) + \widetilde{B^T}(\boldsymbol{\theta})\tilde{B}(\boldsymbol{\theta})) \\ &= (\lambda+G)\left(\left(-\frac{G}{\lambda+G}\widetilde{\Delta_v}(\boldsymbol{\theta}) + \frac{h^2}{4}\tilde{J}(\boldsymbol{\theta})\right) + \widetilde{B^T}(\boldsymbol{\theta})\tilde{B}(\boldsymbol{\theta})\right),\end{aligned} \tag{39}$$

where $\tilde{\Delta}_v(\boldsymbol{\theta}) = \begin{pmatrix} -\frac{4}{h^2}(s_1+s_2) & \\ & -\frac{4}{h^2}(s_1+s_2) \end{pmatrix}$ and $\tilde{J}(\boldsymbol{\theta}) = \begin{pmatrix} \frac{16s_1^2}{h^4} & \\ & \frac{16s_2^2}{h^4} \end{pmatrix}$ are the Fourier symbols of operators $\Delta_v = \begin{pmatrix} \Delta & \\ & \Delta \end{pmatrix}$ and $J = \begin{pmatrix} \partial_{xxxx} & \\ & \partial_{yyyy} \end{pmatrix}$, with ∂_{xxxx} and ∂_{yyyy} the standard discretization of the fourth order derivative with respect to x and y, respectively.

Instead of computing the symbol of A^{-1}, we first consider the symbol of Y^{-1}. $\widetilde{Y^{-1}}(\boldsymbol{\theta})$ can be calculated by applying the Sherman-Morrison-Woodbury formula,

$$\begin{aligned}\widetilde{Y^{-1}}(\boldsymbol{\theta}) &= (\tilde{N}(\boldsymbol{\theta}) + \widetilde{B^T}(\boldsymbol{\theta})\tilde{B}(\boldsymbol{\theta}))^{-1} \\ &= \widetilde{N^{-1}}(\boldsymbol{\theta}) - \widetilde{N^{-1}}(\boldsymbol{\theta})\widetilde{B^T}(\boldsymbol{\theta}) \\ &\quad (I + \tilde{B}(\boldsymbol{\theta})\widetilde{N^{-1}}(\boldsymbol{\theta})\widetilde{B^T}(\boldsymbol{\theta}))^{-1}\tilde{B}(\boldsymbol{\theta})\widetilde{N^{-1}}(\boldsymbol{\theta}),\end{aligned} \tag{40}$$

and therefore

$$\begin{aligned}\tilde{B}(\boldsymbol{\theta})\widetilde{Y^{-1}}(\boldsymbol{\theta})\widetilde{B^T}(\boldsymbol{\theta}) &= \tilde{B}(\boldsymbol{\theta})\widetilde{N^{-1}}(\boldsymbol{\theta})\widetilde{B^T}(\boldsymbol{\theta}) - \tilde{B}(\boldsymbol{\theta})\widetilde{N^{-1}}(\boldsymbol{\theta})\widetilde{B^T}(\boldsymbol{\theta}) \\ &\quad (I + \tilde{B}(\boldsymbol{\theta})\widetilde{N^{-1}}(\boldsymbol{\theta})\widetilde{B^T}(\boldsymbol{\theta}))^{-1}\tilde{B}(\boldsymbol{\theta})\widetilde{N^{-1}}(\boldsymbol{\theta})\widetilde{B^T}(\boldsymbol{\theta}).\end{aligned} \tag{41}$$

TABLE 4 Three-dimensional results - factors predicted by LFA and the asymptotic convergence factors with different number of pre- and post-smoothing steps (ν_1 and ν_2, respectively) and for different values of κ

	(1,0)			(1,1)			(2,1)			(2,2)		
κ	$\mu^{\nu_1+\nu_2}$	ρ	ρ_h	$\mu^{\nu_1+\nu_2}$	ρ	ρ_h	$\mu^{\nu_1+\nu_2}$	ρ	ρ_h	$\mu^{\nu_1+\nu_2}$	ρ	ρ_h
1	0.71	0.71	0.70	0.51	0.51	0.49	0.36	0.36	0.35	0.26	0.26	0.24
10^{-3}	0.71	0.71	0.70	0.51	0.51	0.49	0.36	0.36	0.35	0.26	0.26	0.24
10^{-6}	0.70	0.70	0.68	0.49	0.49	0.47	0.34	0.34	0.33	0.24	0.24	0.22
10^{-10}	0.55	0.55	0.54	0.30	0.30	0.29	0.16	0.17	0.17	0.09	0.12	0.11
0	0.55	0.55	0.54	0.30	0.30	0.29	0.17	0.17	0.17	0.09	0.12	0.11

Denoting $X = \tilde{B}(\boldsymbol{\theta})\widetilde{N^{-1}}(\boldsymbol{\theta})\widetilde{B^T}(\boldsymbol{\theta})$, then

$$\tilde{B}(\boldsymbol{\theta})\widetilde{Y^{-1}}(\boldsymbol{\theta})\widetilde{B^T}(\boldsymbol{\theta}) = X - X(1+X)^{-1}X = \frac{X}{1+X}. \tag{42}$$

We would like to compute X, based on the symbol of N, that is,

$$\begin{aligned}\tilde{\mathrm{N}}(\boldsymbol{\theta}) &= \frac{G}{\lambda+G}\begin{pmatrix} \frac{4}{h^2}(s_1+s_2) & \\ & \frac{4}{h^2}(s_1+s_2)\end{pmatrix} + \frac{h^2}{4}\begin{pmatrix} \frac{16}{h^4}s_1^2 & \\ & \frac{16}{h^4}s_2^2\end{pmatrix} \\ &= \frac{4}{h^2}\begin{pmatrix} \frac{G}{\lambda+G}(s_1+s_2)+s_1^2 & \\ & \frac{G}{\lambda+G}(s_1+s_2)+s_2^2\end{pmatrix},\end{aligned} \tag{43}$$

and subsequently

$$\widetilde{N^{-1}}(\boldsymbol{\theta}) = \frac{h^2}{4}\begin{pmatrix} \frac{\lambda+G}{G(s_1+s_2)+(\lambda+G)s_1^2} & \\ & \frac{\lambda+G}{G(s_1+s_2)+(\lambda+G)s_2^2}\end{pmatrix}. \tag{44}$$

By computing the symbol of B and B^T, we can write

$$\begin{aligned}X &= \left(\frac{-i\sin\theta_1}{h}, \frac{-i\sin\theta_2}{h}\right)\widetilde{N^{-1}}(\boldsymbol{\theta})\begin{pmatrix}\frac{i\sin\theta_1}{h}\\ \frac{i\sin\theta_2}{h}\end{pmatrix} \\ &= (\lambda+G)\left(\frac{s_1\,(1-s_1)}{G(s_1+s_2\,)+(\lambda+G)s_1^2}\right. \\ &\qquad \left. + \frac{s_2(1-s_2)}{G(\,s_1+\,s_2)+\,(\,\lambda+G)s_2^2}\right).\end{aligned} \tag{45}$$

With the relations above, we get

$$\tilde{B}(\boldsymbol{\theta})\widetilde{A^{-1}}(\boldsymbol{\theta})\widetilde{B^T}(\boldsymbol{\theta}) = \frac{1}{\lambda+G}\tilde{B}(\boldsymbol{\theta})\widetilde{Y^{-1}}(\boldsymbol{\theta})\widetilde{B^T}(\boldsymbol{\theta}) = \frac{1}{\lambda+G}\frac{X}{1+X}. \tag{46}$$

With the symbol of C given by $\tilde{C}(\boldsymbol{\theta}) = \frac{s_1+s_2}{\lambda+2G} + \frac{4\kappa}{h^2}(s_1+s_2)$, the following symbol of the Schur complement is obtained,

$$\begin{aligned}\tilde{S}(\boldsymbol{\theta}) &= \tilde{C}(\boldsymbol{\theta}) + \tilde{B}(\boldsymbol{\theta})\widetilde{A^{-1}}(\boldsymbol{\theta})\widetilde{B^T}(\boldsymbol{\theta}) \\ &= \frac{4\kappa(s_1+s_2)}{h^2} + \frac{s_1+s_2}{\lambda+2G} + \frac{1}{\lambda+G}\frac{X}{1+X},\end{aligned} \tag{47}$$

with X from 45. We obtain $\beta_{\max}$ and $\beta_{\min}$ as the maximum and minimum of $\tilde{S}(\boldsymbol{\theta})$ in the high frequencies. Based on 24, an optimal τ minimizing the smoothing factor is given by $\tau = \frac{2\kappa_\beta}{1+\kappa_\beta}$. Relaxation parameter ω has the same expression as in 28.

Approximation. From 47, it is nontrivial to obtain a closed formula for the maximum and minimum eigenvalues of the Schur complement. However, we find by using a sufficiently fine computational grid in the frequency space that these values for the high frequencies can be accurately expressed as,

$$\beta_{\max}(h) \approx \frac{8\kappa}{h^2} + \frac{2}{\lambda+2G} \quad \text{(achieved for } \theta_1 = \theta_2 = \pi\text{)}, \tag{48}$$

$$\beta_{\min}(h) \approx \frac{2\kappa}{h^2} + \frac{1}{\lambda+2G} \quad \text{(achieved for } \theta_1 = 0,\ \theta_2 = \pi/2\text{)}. \tag{49}$$

The eigenvalues of $\frac{1}{\lambda+G}\frac{X}{1+X}$ are small compared with the eigenvalues of C. We have checked the eigenvalues numerically and the maximum and minimum values are identical to the expressions 48 and 49. Taking into account these approximations, we can write

$$\kappa_\beta = \frac{\beta_{\max}(h)}{\beta_{\min}(h)} \approx \frac{8\kappa(\lambda+2G)+2h^2}{2\kappa(\lambda+2G)+h^2}, \tag{50}$$

and in the limit case, when $\kappa = 0$, the simplified expression reads $\kappa_\beta = 2$. With an optimal τ value,

$$\tau = \frac{2\kappa_\beta}{1+\kappa_\beta} \approx \frac{16\kappa(\lambda+2G)+4h^2}{10\kappa(\lambda+2G)+3h^2}, \tag{51}$$

the smoothing factor is found to be

$$\mu_S(h) = \tau - 1 \approx \frac{6\kappa(\lambda+2G)+h^2}{10\kappa(\lambda+2G)+3h^2}.$$

If $\kappa = 0$, then $\mu_S = 1/3$, independently of h, whereas if $\kappa \neq 0$, then $\mu_S = 0.6$, for h sufficiently small. Therefore, we can write

$$\mu_S = \sup_{h\leq h_0} \mu_S(h) = 0.6,$$

independently of the values of κ and the Lamé coefficients λ and G. From 28, 48, and 49, the expression of ω approximately reads

$$\omega = \frac{2h^2(\lambda+2G)}{10\kappa(\lambda+2G)+3h^2}. \tag{52}$$

Obviously, ω is dependent on the mesh size, and the relaxation parameter needs to be determined on each level of the grid. The limit case $\kappa = 0$ yields $\tau = 4/3$, $\mu_S = 1/3$ and $\omega = 2/3(\lambda+2G)$.

Numerical results. Table 5 shows the values of the parameters for the computation of the smoothing factors μ_S and relaxation parameters $\omega > 0$ for different values of the parameter κ, when $h = \frac{1}{256}$ (fixed).

We are also interested in the smoothing factor of the SGS method μ_A of the elasticity operator on the collocated grid.

TABLE 5 Values of the parameters computed by the theory, together with the resulting smoothing factors μ_S when $h = \frac{1}{256}$ on a collocated grid

Parameters	$\kappa = 1$	$\kappa = 10^{-3}$	$\kappa = 10^{-6}$	$\kappa = 10^{-10}$	$\kappa = 0$
$\beta_{\max}$	5.24×10^{5}	524.28	0.52	1.21×10^{-4}	6.86×10^{-5}
$\beta_{\min}$	1.31×10^{5}	131.07	0.13	4.74×10^{-5}	3.43×10^{-5}
κ_β	4	4	4	2.55	2
τ	1.6	1.6	1.6	1.44	1.33
ω	3.05×10^{-6}	3.05×10^{-3}	3.05	11877	19444
μ_S	0.6	0.6	0.6	0.44	0.33

TABLE 6 Relaxation parameters ω on different levels of the grid hierarchy

mesh size	$\kappa = 10^{-3}$	$\kappa = 10^{-6}$	$\kappa = 10^{-7}$	$\kappa = 10^{-8}$
$h = \frac{1}{512}$	7.63×10^{-4}	7.60×10^{-1}	7.63×10^{0}	7.60×10^{1}
$h = \frac{1}{256}$	3.05×10^{-3}	3.05×10^{0}	3.05×10^{1}	3.00×10^{2}
$h = \frac{1}{128}$	1.22×10^{-2}	1.22×10^{1}	1.21×10^{2}	1.15×10^{3}

TABLE 7 Comparison results – factors predicted by LFA and the asymptotic convergence factors with different number of pre- and post-smoothing steps ($\nu_1$and ν_2, respectively) and for different values of κ

	(1,0)			(1,1)		
κ	$\mu^{\nu_1+\nu_2}$	ρ	ρ_h	$\mu^{\nu_1+\nu_2}$	ρ	ρ_h
10^{-3}	0.60	0.60	0.60	0.36	0.36	0.36
10^{-6}	0.60	0.60	0.60	0.36	0.36	0.36
10^{-8}	0.60	0.60	0.59	0.35	0.35	0.38

This value can be computed by LFA, giving $\mu_A = 0.47$ and therefore $(\mu_A)^{1/2} = 0.68$. Because μ_S is smaller, we get a bound $\bar{\mu}$ for the smoothing factor of the whole system from 24, as $\bar{\mu} = \max(0.68, \mu_S) = 0.68$. The upper bound on the smoothing factor is determined by the smoother considered for the displacements in this case.

As commented before, the relaxation parameter ω has to be determined on each grid of the hierarchy. Table 6 shows the values of ω from 52 for different values of the mesh size h and permeability κ. In this table, only results for three grid sizes are presented for simplicity.

Next, with a fixed value of $\kappa = 10^{-6}$, we analyze the performance of the Uzawa smoother for the collocated discretization of the poroelasticity system. For different sizes of the finest grid, the LFA smoothing factor μ for the whole system together with the two-grid convergence factor ρ predicted by LFA with only one smoothing step are given by $\mu = \rho = 0.60$ in all cases, using ω as in Table 6.

We also consider the numerical multigrid convergence. The performance of the multigrid algorithm and the results predicted by LFA are compared in Table 7. The actual multigrid convergence factors ρ_h are obtained when the residual is reduced to 10^{-20} in maximum norm. The results are shown for different numbers of smoothing steps ((1,0) and (1,1)) and using the relaxation parameters ω as in Table 6. The numerical multigrid results are computed for F-cycles on a grid with $h = \frac{1}{256}$. The numerical experiments show that the asymptotic multigrid convergence factors ρ_h accurately resemble the LFA two-grid convergence factors ρ.

We also confirm the h-independent convergence behavior of the multigrid method. For $\kappa = 10^{-3}$ and a multigrid $F(1,1)-$cycle, computing on different meshes with $h = 1/2^k$, $k = 6,7,8,9$, the multigrid convergence factor is around 0.22 for all cases, and the multigrid method exhibits a highly satisfactory behavior.

We wish to check the sensitivity of the multigrid convergence with respect to the exact choice of the relaxation parameter ω. Supposing ω has already been obtained from 52 on each level ($h = \frac{1}{128}$ being the finest grid here), the convergence behavior of the multigrid is plotted in Figure 3 (dashed line). However, we can also simply round the significant digits of ω to the nearest integer number, while leaving the exponent part unchanged. For example, instead of $\omega = 7.63 \cdot 10^{-4}$ in Table 6, we use 'the inexact value' $\omega = 8 \cdot 10^{-4}$. The convergence with the inexact parameter is denoted by asterisks in Figure 3. There is no significant difference between the multigrid convergence results with exact parameters and those with these inexact parameters. To improve the convergence performance, the iterant recombination scheme as presented in Section 3.1, can be employed. The acceleration scheme with either exact or inexact ω are denoted by crosses and circles, respectively. The results show a highly satisfactory convergence performance in Figure 3.

The deviation from the 'exact' value of ω can be assessed by LFA too. In Figure 4, we show the two-grid convergence factors predicted by LFA with respect to the ratio between the 'inexact' value of ω and 'exact' optimal ω, for the case $\kappa = 10^{-6}$. Similar pictures are obtained for other values of the permeability.

Some more numerical tests in which we consider Uzawa parameters for non-square meshes are discussed in Appendix A.2.

5.3 | Heterogeneity case (for collocated grids)

In this section, we consider the poroelasticity system with heterogeneous coefficients. Heterogeneity is a concept related to nonuniformity (composition or character) in a substance. Usually, materials have complicated properties and they are assumed to be a heterogeneous deformable body composed of different materials. The heterogeneity can influence the poroelastic behavior in many ways. We wish to consider the effect of heterogeneity on the multigrid convergence.

It is known that anisotropy is one of the complicating factors which can influence the multigrid convergence behavior.

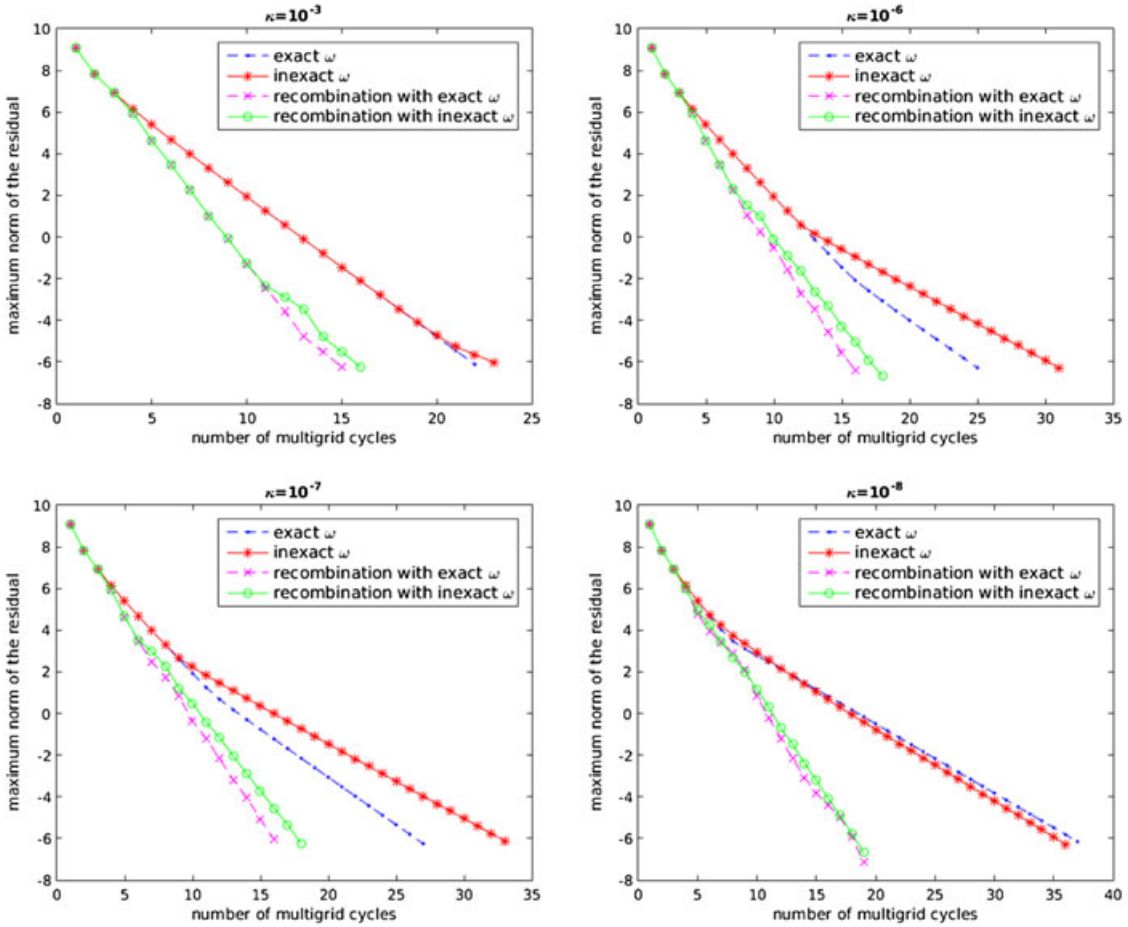

FIGURE 3 Sensitivity regarding the choice of ω when $h = \frac{1}{128}$ for different values of the permeability.

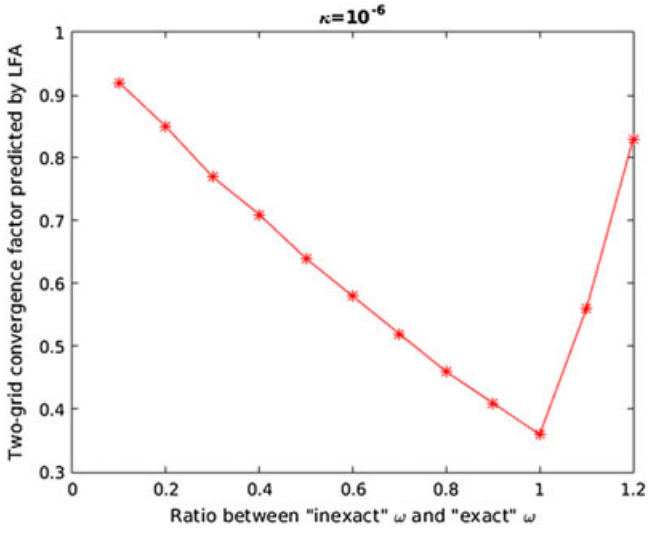

FIGURE 4 Two-grid convergence factors predicted by LFA for different choices of 'inexact' ω and $\kappa = 10^{-6}$.

To improve the convergence performance, we consider the acceleration scheme for multigrid as in Section 3.1.

Weibull distribution. In order to simulate the heterogeneity in a solid material, a statistical approach is used. The heterogeneity is defined by a Weibull distribution, with probability density function given by

$$f(s,m) = \frac{m}{\bar{s}}\left(\frac{s}{\bar{s}}\right)^{m-1} \exp\left(-\left(\frac{s}{\bar{s}}\right)^{m}\right), \tag{53}$$

where s denotes a given coefficient, such as the Lamé coefficients or the permeability; $\bar{s}$ is the mean value; and m represents the homogeneity index which defines the shape of the distribution function. The use of Equation 53 to simulate the heterogeneity in a solid material is presented in[19] and.[20] Figure 5 displays, for different values of the homogeneity index m, the probability density function in terms of the ratio between s and $\bar{s}$. It is obvious that a higher value of m represents more homogeneous material and vice versa, as for higher m, the values of s are concentrated around $\bar{s}$.

In a multigrid algorithm, the material properties need to be transferred to coarse grids. In this way, the coarse system is related to the fine system, so that the same characteristics of the material are guaranteed. Lamé coefficients and the permeability are restricted to each grid level by full weighting operators. Then, we perform a regular finite volume discretization with these averaged coefficients on the coarse grids. The highly varying properties cannot represent the original material on coarse grids accurately. We wish to study the impact of the heterogeneity on the multigrid convergence using the standard multigrid components described above on a collocated grid.

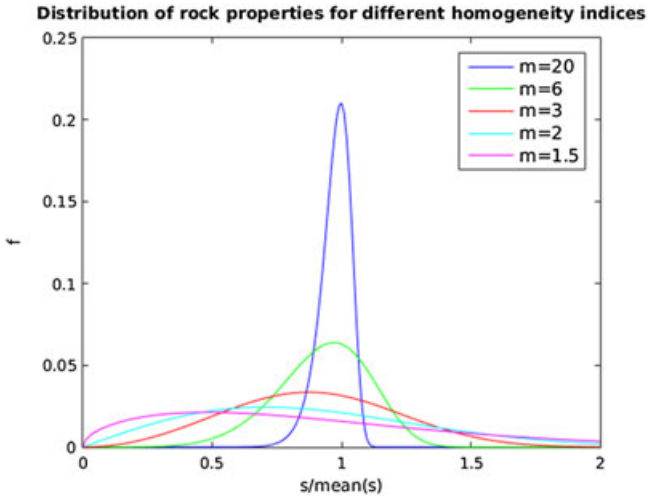

FIGURE 5 Density function.

TABLE 8 Convergence factors (and number of iterations between brackets) of multigrid method and multigrid with iterant recombination for a heterogeneous test. ('/' denotes divergence)

index	scheme	$\kappa = 10^{-3}$	$\kappa = 10^{-6}$	$\kappa = 10^{-7}$	$\kappa = 10^{-8}$
$m = 10$	Multigrid	0.24(23)	0.28(25)	0.30(27)	0.43(38)
	Acc Multigrid	0.12(15)	0.13(16)	0.14(17)	0.17(19)
$m = 5$	Multigrid	0.25(24)	0.28(26)	0.31(27)	0.43(38)
	Acc Multigrid	0.12(16)	0.14(17)	0.15(17)	0.19(19)
$m = 3$	Multigrid	0.28(26)	0.29(26)	0.31(28)	0.42(37)
	Acc Multigrid	0.13(16)	0.16(18)	0.19(20)	0.24(23)
$m = 2$	Multigrid	0.31(28)	0.31(28)	0.38(34)	/
	Acc Multigrid	0.15(18)	0.24(23)	0.28(26)	0.69(93)

Comparison test. In Table 8, for different homogeneity indices and permeabilities, the numerical multigrid convergence factors for an F-cycle with one pre- and one post-smoothing step are presented. The values in parentheses are the numbers of multigrid iterations needed to reduce the residual to 10^{-6} in maximum norm. All results are obtained on a grid with $h = \frac{1}{128}$. Notice that the relaxation parameters ω are varied in the computational domain for the heterogeneity case, because ω is related to the stochastically distributed Lamé coefficients and permeability. Multigrid does not converge for very small homogeneity index, such as $m = 1$. This is due to the heterogeneity properties of the material and the choice of multigrid components here. For the problems with strongly 'varying' coefficients, Galerkin coarse matrices, operator-dependent prolongation and restriction should be considered, see (,[10] Chapter 7).

To illustrate the efficiency of the acceleration method proposed in Section 3.1, Table 8 also shows the convergence results with multigrid acceleration by iterant recombination denoted as 'Acc Multigrid'. All the initial settings in this numerical test are the same as in 'Multigrid' without acceleration. When the acceleration scheme is applied, $\tilde{q}$ is 5. Obviously, the convergence behavior corresponding to 'Multigrid' is nicely improved by the iterant recombination for each heterogeneity case. The additional work required for 'Acc Multigrid' is negligible.

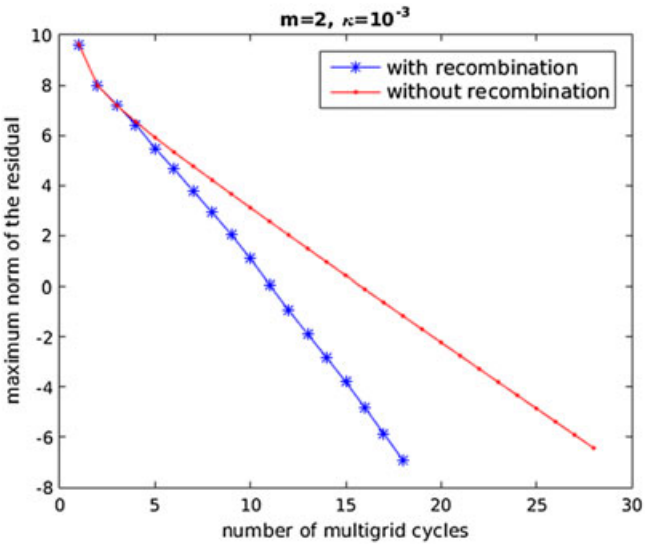

FIGURE 6 Comparison results between the history of the convergence for multigrid method and iterant recombination scheme.

We consider an extreme case where the homogeneity index is two and the coefficient of permeability is 10^{-3}. Figure 6 plots the decreasing residuals with respect to multigrid iterations. The errors are plotted in logarithmic scale. It can be seen that it takes fewer multigrid cycles for the acceleration scheme to reach a same residual tolerance. The CPU time is also compared. The cost of iterant recombination is less than the cost of standard multigrid to solve the problem. Based on the discussions above, the robustness of the iterant recombination is confirmed. For complicated problems, the recombination technique may give a more prominent acceleration performance.

6 | CONCLUSION

In this paper, we focused on an efficient multigrid method for the poroelasticity equations from Biot's model of consolidation. A decoupled smoother called Uzawa smoother is chosen in the multigrid algorithm. It involves a SGS smoothing for displacements and a simple Richardson iteration for the Schur complement regarding the pressure field. In order to select an optimal relaxation parameter in the Richardson iteration, LFA is applied. The convergence performance can also be predicted in the framework of LFA. Numerical tests confirm our theoretical analysis. At the same time, some problems towards engineering applications are considered. We use the iterant recombination scheme for the heterogeneous poroelasticity equations. It is demonstrated that the convergence factors are nicely improved by this scheme in many cases.

ACKNOWLEDGMENT

Peiyao Luo is grateful for the financial support by the China Scholarship Council (CSC) and NDNS+PhD travel grant.

The research of Carmen Rodrigo has been partially supported by FEDER/MCYT Projects MTM2013-40842-P and the DGA (Grupo consolidado PDIE). Francisco Gaspar and Cornelis Oosterlee have received funding from the European Union's Horizon 2020 research and innovation programme under the Marie Sklodowska-Curie grant agreement no. 705402, POROSOS.

How to cite this article: Luo, P., Rodrigo, C., Gaspar, F. J., and Oosterlee, C. W. (2017) On an Uzawa smoother in multigrid for poroelasticity equations. *Numer Linear Algebra Appl*, 24, e2074. doi:10.1002/nla.2074

REFERENCES

1. Venkatramaiah C. Geotechnical Engineering. New Delhi: New Age International; 2006.
2. Biot MA. General theory of three-dimensional consolidation. J Appl Phys. 1941;12(2):155–164.
3. Biot MA. Theory of elasticity and consolidation for a porous anisotropic solid. J Appl Phys. 1955;26(2):182–185.
4. Gaspar FJ, Lisbona FJ, Oosterlee CW. A stabilized difference scheme for deformable porous media and its numerical resolution by multigrid methods. Comput Visual Sci. 2008;11(2):67–76.
5. Oosterlee CW, Gaspar FJ. Multigrid relaxation methods for systems of saddle point type. Appl Numer Math. 2008;58(12):1933–1950.
6. Gaspar FJ, Lisbona FJ, Oosterlee CW, Wienands R. A systematic comparison of coupled and distributive smoothing in multigrid for the poroelasticity system. Numer Linear Algebra Appl. 2004;11(2-3):93–113.
7. Vanka SP. Block-implicit multigrid solution of Navier-Stokes equations in primitive variables. J Comput Phys. 1986;65(1):138–158.
8. Maitre JF, Musy F, Nigon P. A fast solver for the Stokes equations using multigrid with a Uzawa smoother. Advances in multi-grid methods. Berlin: Springer; 1985. p.77–83.
9. Gaspar FJ, Notay Y, Oosterlee CW, Rodrigo C. A simple and efficient segregated smoother for the discrete Stokes equations. SIAM J Sci Comput. 2014;36(3):A1187–A1206.
10. Trottenberg U, Oosterlee CW, Schuller A. Multigrid. London: Academic Press; 2000.
11. Brandt A. Multi-level adaptive solutions to boundary-value problems. Math Comp. 1977;31(138):333–390.
12. Brandt A. Rigorous quantitative analysis of multigrid, I. constant coefficients two-level cycle with L2-norm. SIAM J Sci Comput. 1994;31(6):1695–1730.
13. Wesseling P. Introduction to multigrid methods. Virginia: DTIC Document; 1995. Technical report.
14. Wienands R, Joppich W. Practical Fourier analysis for multigrid methods. New York: CRC Press; 2004.
15. Washio T, Oosterlee CW. Krylov subspace acceleration for nonlinear multigrid schemes. Electron T Numer Ana. 1997;6(271-290):3–1.
16. Axelsson O. Iterative solution methods. Cambridge: Cambridge University Press; 1996.
17. MacLachlan SP, Oosterlee CW. Local fourier analysis for multigrid with overlapping smoothers applied to systems of PDEs. Numer Linear Algebra Appl. 2011;18(4):751–774.
18. Gaspar FJ, Gracia JL, Lisbona FJ, Oosterlee CW. Distributive smoothers in multigrid for problems with dominating grad–div operators. Numer Linear Algebra Appl. 2008;15(8):661–683.
19. Tang C, Liu H, Lee PKK, Tsui Y, Tham LG. Numerical studies of the influence of microstructure on rock failure in uniaxial compression, part I: Effect of heterogeneity. Int J Rock Mech Min Sci. 2000;37(4):555–569.
20. Yang T, Tham LG, Tang C, Liang Z, Tsui Y. Influence of heterogeneity of mechanical properties on hydraulic fracturing in permeable rocks. Rock Mech Rock Eng. 2004;37(4):251–275.

APPENDIX

A. Non-square meshes

In this Appendix, we detail the extension of the proposed analysis for the Uzawa-based multigrid method to the case in which the grid has different horizontal and vertical mesh sizes h_x and h_y. Next, we describe the analysis for both staggered and collocated meshes.

A.1 Staggered grid arrangement of unknowns

When the mesh size in x-direction h_x is not equal to the size in y-direction h_y, it is not immediately clear which parameter ω should be used. The symbol of $-\Delta$ is in this case,

$$-\tilde{\Delta}(\boldsymbol{\theta}) = 4\left(\frac{s_1}{h_x^2} + \frac{s_2}{h_y^2}\right). \tag{A1}$$

From 31 and A1, the symbol of the Schur complement S equals

$$\tilde{S}(\boldsymbol{\theta}) = 4\kappa\left(\frac{s_1}{h_x^2} + \frac{s_2}{h_y^2}\right) + \frac{1}{\lambda + 2G}. \tag{A2}$$

The maximum eigenvalue of $-\Delta$ is achieved when $s_1 = s_2 = 1$, then

$$\beta_{\max}(h) = 4\kappa\left(\frac{1}{h_x^2} + \frac{1}{h_y^2}\right) + \frac{1}{\lambda + 2G}. \tag{A3}$$

The minimum value of $-\Delta$ results to be $\frac{2\kappa}{h_y^2}$ if $h_y > h_x$ (for $s_1 = 0, s_2 = \frac{1}{2}$) or $\frac{2\kappa}{h_x^2}$ otherwise (for $s_1 = \frac{1}{2}$ and $s_2 = 0$). Therefore, $\beta_{\min}(h)$ becomes

$$\begin{aligned}\beta_{\min}(h) &= 2\kappa \min\left\{\frac{1}{h_x^2}, \frac{1}{h_y^2}\right\} + \frac{1}{\lambda + 2G} \\ &= \frac{2\kappa}{\max\left\{h_x^2, h_y^2\right\}} + \frac{1}{\lambda + 2G}.\end{aligned} \tag{A4}$$

To compute $\kappa_\beta = \frac{\beta_{\max}}{\beta_{\min}}$ using A3 and A4, we have that

$$\kappa_\beta = \begin{cases} \frac{h_x^2 h_y^2 + 4\kappa(h_x^2 + h_y^2)(\lambda + 2G)}{h_x^2 h_y^2 + 2\kappa(\lambda + 2G)h_y^2}, \text{when} \quad h_x > h_y, \\ \frac{h_x^2 h_y^2 + 4\kappa(h_x^2 + h_y^2)(\lambda + 2G)}{h_x^2 h_y^2 + 2\kappa(\lambda + 2G)h_x^2}, \text{when} \quad h_x < h_y. \end{cases}$$

Therefore,

$$\kappa_\beta = \frac{h_x^2 h_y^2 + 4\kappa(h_x^2 + h_y^2)(\lambda + 2G)}{h_x^2 h_y^2 + 2\kappa(\lambda + 2G)\min\{h_x^2, h_y^2\}}. \tag{A5}$$

TABLE A1 Values of ω,ρ predicted by LFA when $h_x \neq h_y$ on a staggered grid

$h_x = \frac{1}{128}$				
mesh		$h_y = \frac{1}{64}$	$h_y = \frac{1}{128}$	$h_y = \frac{1}{256}$
LFA	ω	22.17	12.20	5.55
	ρ	0.67	0.38	0.69

Assuming $h_x > h_y$ for the following analysis, we choose the optimal τ giving the lowest value of the maximum from 24,

$$\tau = \frac{2\kappa_\beta}{1+\kappa_\beta} = \frac{h_x^2h_y^2 + 4\kappa(\lambda+2G)(h_x^2+h_y^2)}{h_x^2h_y^2 + 3\kappa(\lambda+2G)h_y^2 + 2\kappa(\lambda+2G)h_x^2}. \tag{A6}$$

In this way, the relaxation parameter can be obtained by substituting A3 and A4 in the expression of ω in 38,

$$\omega = \frac{2}{\beta_{\max}+\beta_{\min}} = \frac{1}{\frac{1}{\lambda+2G} + \frac{3\kappa}{h_x^2} + \frac{2\kappa}{h_y^2}}. \tag{A7}$$

By using these relaxation parameters, the smoothing factor can be computed as

$$\mu_S = \tau - 1 = \frac{\kappa(\lambda+2G)(2h_x^2+h_y^2)}{h_x^2h_y^2 + 3\kappa(\lambda+2G)h_y^2 + 2\kappa(\lambda+2G)h_x^2}. \tag{A8}$$

If the grid size is extremely small, the term $h_x^2h_y^2$ can be neglected. The smoothing factor is dominated by the value $\frac{2h_1^2+h_2^2}{3h_2^2+2h_1^2}$. However, for the case $h_x \gg h_y$, the smoothing factor tends to 1. It indicates that when the grid becomes anisotropic, we obtain worse convergence results and appropriate block-wise smoothers or semi-coarsening may be required.

In Table A1, we fix h_x to $\frac{1}{128}$ and gradually change h_y. We have chosen $\kappa = 10^{-6}$ and two smoothing steps. The optimal parameter ω on the finest grid and the two-grid convergence factor ρ predicted from LFA are displayed.

A.2 Collocated grid arrangement of unknowns

Here, we will analyze the case where the collocated grid has different horizontal and vertical mesh sizes h_x and h_y. We have $C = -\kappa\Delta - \frac{h_x^2}{4(\lambda+2G)}\partial_{xx} - \frac{h_y^2}{4(\lambda+2G)}\partial_{yy}$ with the stabilization term. The symbols of ∂_{xx} and ∂_{yy} are $-\frac{4s_1}{h_x^2}, -\frac{4s_2}{h_y^2}$, and

$$\tilde{C}(\boldsymbol{\theta}) = 4\kappa\left(\frac{s_1}{h_x^2} + \frac{s_2}{h_y^2}\right) + \frac{s_1+s_2}{\lambda+2G}.$$

Subsequently, the symbol of the Schur complement is given by

$$\begin{aligned}\tilde{S}(\boldsymbol{\theta}) &= \tilde{C}(\boldsymbol{\theta}) + \tilde{B}(\boldsymbol{\theta})\widetilde{A^{-1}}(\boldsymbol{\theta})\widetilde{B^T}(\boldsymbol{\theta}) \\ &= 4\kappa\left(\frac{s_1}{h_x^2} + \frac{s_2}{h_y^2}\right) + \frac{s_1+s_2}{\lambda+2G} + \frac{1}{\lambda+G}\frac{X}{1+X},\end{aligned}$$

TABLE A2 Convergence factors (and number of iterations between brackets) corresponding to multigrid (ρ_h) and to the iterant recombination technique ($\rho_{h,acc}$) necessary to reduce the initial residual to 10^{-6} together with values of ω,ρ predicted by LFA when $h_x \neq h_y$

$h_x = \frac{1}{128}$				
mesh		$h_y = \frac{1}{64}$	$h_y = \frac{1}{128}$	$h_y = \frac{1}{256}$
LFA	ω	22.17	12.20	5.55
	ρ	0.67	0.36	0.67
	ρ_h	0.58(58)	0.27(25)	0.60(62)
	$\rho_{h,acc}$	0.28(25)	0.13(16)	0.28(26)

TABLE A3 Convergence factors (and number of iterations between brackets) corresponding to the multigrid ρ_h and to the iterant recombination technique ($\rho_{h,acc}$) necessary to reduce the initial residual to 10^{-6} together with values of ρ predicted by LFA with ω corresponding to $h_x = h_y = \frac{1}{256}$

$h_x = \frac{1}{256}$				
mesh		$h_y = \frac{1}{128}$	$h_y = \frac{1}{192}$	$h_y = \frac{1}{256}$
LFA	ρ	0.81	0.60	0.36
	ρ_h	0.72(99)	0.47(44)	0.26(25)
	$\rho_{h,acc}$	0.36(32)	0.21(22)	0.12(16)

where $X = \tilde{B}(\boldsymbol{\theta})\widetilde{N^{-1}}(\boldsymbol{\theta})\widetilde{B^T}(\boldsymbol{\theta})$ and $\tilde{\mathrm{N}}(\boldsymbol{\theta}) = -\frac{G}{\lambda+G}\widetilde{\Delta_v}(\boldsymbol{\theta}) + \tilde{J}_1(\boldsymbol{\theta})$. Note that $\widetilde{\Delta_v}(\boldsymbol{\theta}) = \begin{pmatrix} -4\left(\frac{s_1}{h_x^2}+\frac{s_2}{h_y^2}\right) & \\ & -4\left(\frac{s_1}{h_x^2}+\frac{s_2}{h_y^2}\right)\end{pmatrix}, \tilde{J}_1(\boldsymbol{\theta}) = \begin{pmatrix} \frac{4s_1^2}{h_x^2} & \\ & \frac{4s_2^2}{h_y^2}\end{pmatrix}$ and $\tilde{B}(\boldsymbol{\theta}) = \left(\frac{-i\sin\theta_1}{h_x}, \frac{-i\sin\theta_2}{h_y}\right)$ are the necessary symbols for computing X. The exact expression of the relaxation parameter ω is not obtained due to the involved expression for the collocated case. So we compute the parameter numerically for non-square meshes.

In the following test, h_x is fixed to $\frac{1}{128}$ and h_y is gradually changed. LFA is applied to compute the optimal parameter ω on the finest grid and predict the two-grid convergence factor ρ. With the obtained ω-values, we employ both the pure multigrid cycles and the iterant recombination scheme mentioned earlier for a homogeneous problem. When the residual is reduced to 10^{-20} in maximum norm, the asymptotic convergence factor ρ_h is well predicted by the two-grid convergence factor ρ. However, in real applications, such a small residual is not necessary. In Table A2, we display the convergence factors and the number of multigrid cycles (in parentheses) needed to reduce the initial residual to 10^{-6} in maximum norm, together with the values of ω and ρ obtained by LFA. The efficiency of the recombination scheme is demonstrated because the observed convergence factors reduce by a factor two compared to those obtained with the multigrid cycle. Obviously, the convergence factor $\rho_{h,acc}$ is much smaller than ρ_h for all cases.

In Table A3, the same test as in Table A2 is performed, with the only difference that we use non-optimal parameters associated with $h_x = h_y = \frac{1}{256}$ for all the cases in Table A3.

We observe that the convergence factors become much worse compared to the values in Table A2. This points out the need for a good choice of relaxation parameters.

In addition, we find that if the relaxation parameters corresponding to $h_x = h_y = \frac{1}{128}$ are used for the case $h_x = \frac{1}{256}, h_y = \frac{1}{128}$, the algorithm does not converge. The value of ω depends on the minimum size of the grid. Therefore, for the test $\frac{1}{256} = h_x < h_y = \frac{1}{128}$, the parameter with respect to the smaller size h_x should be considered. The convergence performance is described in Table A3. Again, LFA can predict the asymptotic convergence factor (not shown in the table) accurately and the recombination scheme indeed improves the efficiency. When $h_x \neq h_y$ and even the optimal parameters are not available, we can use the parameters that correspond to the minimum of h_x and h_y.